Journal of Alloys and Compounds xxx (xxxx) xxx

Contents lists available at ScienceDirect

Journal of Alloys and Compounds

journal homepage: http://www.elsevier.com/locate/jalcom

Comparative spectroscopic studies of MOCVD grown AlN films on Al_2O_3 and 6H–SiC

Junhua Yin [a, b], Daihua Chen [a], Hong Yang [a], Yao Liu [a], Devki N. Talwar [c], Tianlong He [a], Ian T. Ferguson [d], Kaiyan He [a, **], Lingyu Wan [a, b], Zhe Chuan Feng [a, b, *]

[a] *Laboratory of Optoelectronic Materials & Detection Technology, Center on Nano-Energy Research, Guangxi Key Laboratory for the Relativistic Astrophysics, School of Physical Science & Technology, Guangxi University, Nanning, 530004, China*
[b] *State Key Laboratory of Luminescence and Applications, Changchun Institute of Optics, Fine Mechanics and Physics, Chinese Academy of Sciences, Changchun, 130033, China*
[c] *Department of Physics, University of North Florida, Jacksonville, FL, 32224, USA*
[d] *Southern Polytechnic College of Engineering and Engineering Technology, Kennesaw University, Kennesaw, GA, 30144, USA*

ARTICLE INFO

Article history:
Received 2 September 2020
Received in revised form
4 October 2020
Accepted 6 October 2020
Available online xxx

Keywords:
Aluminum nitride
Sapphire
6H–SiC
Photoluminescence (PL)
X-ray photoelectron spectroscopy (XPS)
Temperature-dependent Raman

ABSTRACT

A comprehensive spectroscopic study is reported for MOCVD (Metal organic chemical vapor deposition) grown AlN thin films prepared on sapphire (Al_2O_3) and 6H–SiC substrates. Impacts of substrate on the structural, surface and optical properties of AlN epilayers are meticulously appraised by using high resolution X-ray diffraction (HR-XRD), X-ray photoelectron spectroscopy (XPS), Raman scattering (RS), optical transmission (OT), spectroscopic ellipsometry (SE), photoluminescence (PL) and atomic force microscopy (AFM). Comparative results with different spectroscopic studies have revealed better crystalline quality of the AlN films grown on 6H–SiC than on Al_2O_3. For AlN/Al_2O_3 our extensive measurements have clearly uncovered a significant influence of the substrate on film's surface roughness, dislocation density, grain size, micro strain and the incorporation of oxygen on its surface. Careful analysis of the temperature-dependent RS results have shown an appealing phenomena of the existing biaxial stress in AlN films altering from compressive to tensile stress as the temperature is increased from 80 K to 800 K. This effect exhibits higher temperature inflection point for AlN/Al_2O_3 film than AlN/6H–SiC.

1. Introduction

Aluminum nitride (AlN) is an important direct wide bandgap ($E_g = 6.2$ eV) semiconductor with high temperature stability, high resistivity (10^{11}-10^{13} Ω-cm), high thermal conductivity (285 W/mK) and high breakdown field ($1.2–1.8 \times 10^6$ V/cm) [1–8]. AlN and related materials are very promising with broader application prospects in the areas of high-density optical data storage, biomedical research, solid-state light sources, and air sterilization [9–16]. The good piezoelectric and related properties of AlN can also be adapted for designing surface acoustic wave devices, laser diodes and light-emitting diodes [17]. Metal organic chemical vapor deposition (MOCVD) is widely used to grow large-area and high-quality III-nitride based epitaxial layers [6–8,15,18,19]. In the absence of suitable substrates, most AlN thin films are heterogeneously grown on sapphire (Al_2O_3) and SiC (Silicon carbide). Sapphire is the most popular substrate for aluminum nitride growth because of its stability at high temperatures and transparency in the ultraviolet band region [6–8,12,13,18,20–24]. Due to a large mismatch in the lattice constant and thermal expansion coefficient (TEC) between AlN and sapphire, the epitaxially grown AlN/Al_2O_3 films usually exhibit a high density of linear misalignment (10^9-$10^{10}cm^{-2}$) [22–25]. The highly stressed epitaxial AlN films generally reveal high threading dislocation density from HR-TEM/STEM on MOCVD-grown AlN/Al_2O_3 [22]. These defects act as non-radiative recombination centers or leakage current paths, which significantly reduce device performance [14]. Using 6H–SiC as a substrate for AlN growth is a good choice [5,26,27]. But some problems may appear as the growth temperature is high, and SiC is

---

* Corresponding author. Laboratory of Optoelectronic Materials & Detection Technology, Center on Nano-Energy Research, Guangxi Key Laboratory for the Relativistic Astrophysics, School of Physical Science & Technology, Guangxi University, Nanning, 530004, China.
** Corresponding author. (K.He).
E-mail addresses: gredhky@gxu.edu.cn (K. He), fengzc@gxu.edu.cn (Z.C. Feng).

https://doi.org/10.1016/j.jallcom.2020.157487
0925-8388/

Please cite this article as: J. Yin, D. Chen, H. Yang *et al.*, Comparative spectroscopic studies of MOCVD grown AlN films on Al_2O_3 and 6H–SiC, Journal of Alloys and Compounds, https://doi.org/10.1016/j.jallcom.2020.157487

easily decomposed with large mismatch between the TEC and lattice constant of AlN and SiC [26]. Cross-sectional TEM/STEM images of 500-nm-thick AlN on 6H–SiC with different V/III ratios had revealed threading dislocation density (TDD) and cracks [5]. Furthermore, research works have been done in the field of AlN epitaxial films grown on different substrates to obtain high-quality AlN epitaxial films, such as Si [28,29], 4H–SiC [30], 3C–SiC [16], and glass [14].

While many investigations on the optical properties of AlN/Al_2O_3 films are reported – only a few studies exist comprehending the characteristics of AlN films prepared on other substrates. Among others, the use of low mechanical loss materials such as single crystal silicon (Si) and 6H–SiC are probably the most compatible substrates with conventional micro-fabrication processes for increasing quality factor, Q of the piezoelectric resonant devices. While the low acoustic velocity of Si substrate has the disadvantage for high frequency devices – the high acoustic velocity of 6H–SiC warrants investigations for enhancing the Q of AlN-based resonant devices without compromising the resonance frequency. This study aims to systematically study the optical and material properties of AlN grown on Al_2O_3 and 6H–SiC substrate.

To comprehend the influence of heterogeneous substrates on surface morphology, crystalline structure and optical properties, which could provide a useful information on device fabrications – we have employed an MOCVD method (cf. Sec. 2) to grow a series of AlN thin films on 6H–SiC and c-plane Al_2O_3 substrates. Several characterization techniques, including high resolution X-ray diffraction (HR-XRD), X-ray photoelectron spectroscopy (XPS), Raman scattering (RS), optical transmission (OT), spectroscopic ellipsometry (SE), photoluminescence (PL) and atomic force microscopy (AFM), are employed (cf. Sec. 3) to comprehensively analyze some valuable properties of AlN epifilms. By exciting the PL spectra with deep-ultraviolet (DUV) 193 nm laser source, we compared the luminescence performance and extracted the band gap E_g of the two AlN films. HR-XRD was used to analyze the structural characteristics of the films, and to understand the differences between their micro-strain, grain size, and dislocation density. We employed XPS to analyze the valence state of the film and the thickness of its surface oxide film. By using a temperature-dependent RS, the spectral line width, stress and E_2 (high) mode were carefully characterized for the AlN films grown on two different substrates. The OT and polarization dependent SE spectra were used to verify the band gap values of the film grown on the sapphire substrate. The transmittance data of the film was analyzed to obtain the film thickness and surface morphology of AlN film studied by AFM.

2. Samples and experiments

Two samples of AlN used in this study were prepared by metal organic chemical vapor deposition (MOCVD) grown on c-plane Al_2O_3 (#F5428 briefly named as Sa) and 6H–SiC (#F5444 briefly named as Sc) substrates. Using the conventional method for the growth of AlN epitaxial layer, we employed trimethyl aluminum (TMA) and ammonia (NH_3) as gas sources, and hydrogen (H_2) as carrier gas at temperatures, typically above 1000 °C. The epifilms were characterized by various spectroscopic techniques including PL, HR-XRD, XPS, Raman scattering, OT, SE and AFM, etc.

By exciting the sample with an extreme DUV laser (193 nm) we analyzed their luminescence performance. The crystal orientation and structure of the sample were characterized by HR-XRD (SMARTLAB3KW) using $Cu_{K\alpha}$ radiation ($\lambda = 0.15406$ nm). We performed 2θ scans in the angle range of 25° -140° with a step size of 0.1° as well as omega scans in the (0002) direction. XPS (ESCALAB 250XI) was used to characterize the composition on the surface of the samples – all XPS binding energies were calibrated to the C 1s peak at 284.8 eV; A program of XPSpeak 4.1 was used for fittings to obtain the binding energies in different chemical states. The RS results were measured by using a micro-Raman spectrometer and different excitation laser sources with wavelengths of 266 nm (FQCW266) and 532 nm (MLL-U-532). We used a UV–visible spectrophotometer (Zolix OmniAs, China) with deuterium lamps.

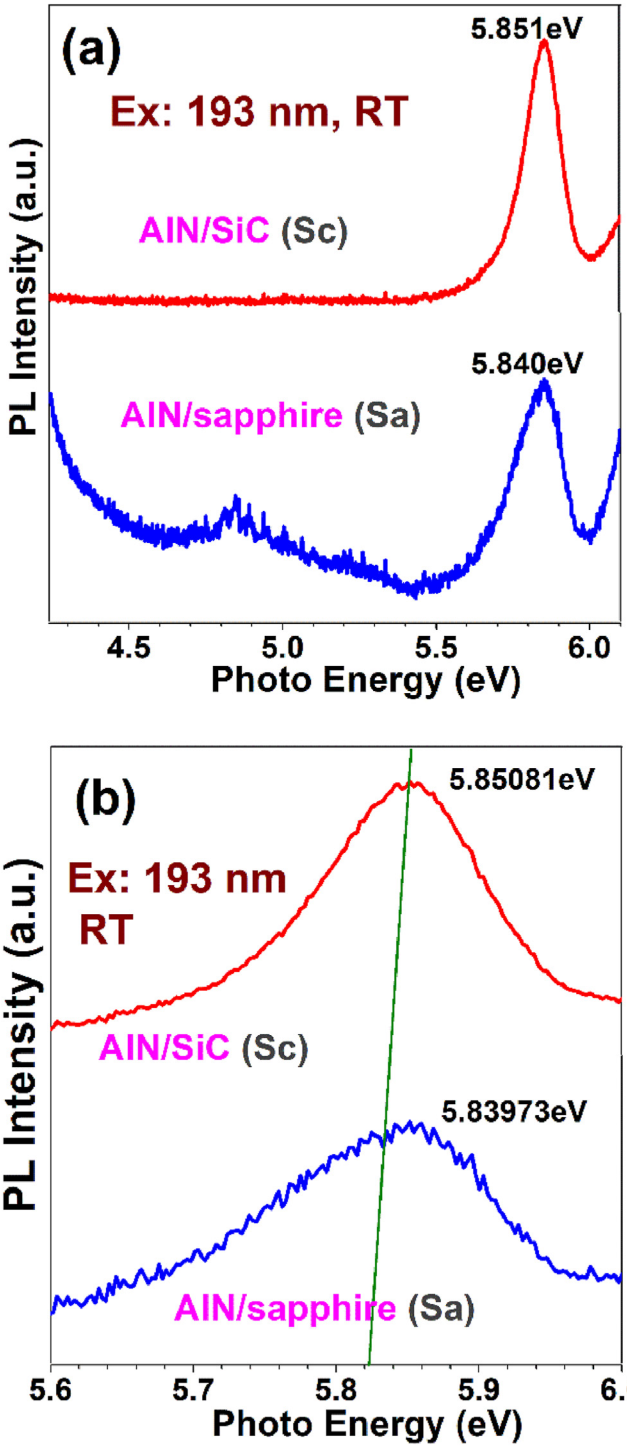

Fig. 1. (a) PL spectra excited by 193 nm laser, (b) Enlarged view, for AlN/SiC (Sc) and AlN/sapphire (Sa), respectively.

The absorption characteristics of AlN films were characterized by OT spectroscopy. The film thickness, roughness and band gap were analyzed using a variable angle ellipsometer (VASE; ME-L ellipsometer, Wuhan Eoptics Technology Co. Ltd. China). The AFM (Dimension Icon) micrographs were taken to comprehend the surface morphology of the samples. All the above measurements were performed at room temperature (RT). Temperature-dependent RS (80 K–800 K) data analysis was performed using Linkam heating system (THMS600) and water circulator with an excitation laser wavelength of 266 nm.

3. Results and discussion

3.1. Structure and composition

3.1.1. Photoluminescence analysis

Fig. 1 shows the DUV fluorescence spectrum of two MOCVD grown AlN samples. The wavelength of the laser that we used here is 193 nm. AlN grown on 6H–SiC has a fluorescence emission peak at 211.9 nm (5.851 eV). The aluminum nitride film grown on sapphire has a fluorescence emission peak at 212.3 nm (5.840 eV) and a weak fluorescence emission peak at 258.7 nm (4.85 eV). The peak at 213.3 nm is its intrinsic emission peak, while the one at 258.7 nm may be caused by the structural anisotropy of AlN. A strong single fluorescence emission peak can be observed in the fluorescence spectrum, which can be explained by the thickness of the film, which is much smaller than the wavelength of the stimulated radiation near the edge of the band [31,32]. Secondly, the fluorescence emission peak also has a slight shift. It can be noted that the aluminum nitride film grown on the sapphire substrate not only has its intrinsic emission peak, but also has an edge emission peak; while the aluminum nitride film grown on the silicon carbide substrate has only its intrinsic emission peak. Therefore, the difference in the fluorescence spectra of the two aluminum nitride films is caused by the stress caused by the difference in the two substrates. The stress in the aluminum nitride films will be described later.

In order to better comprehend the emission spectra we have performed the Gaussian fitting on the PL spectra excited by 193 nm laser. The results are displayed in Fig. 2 with fitting parameters reported in Table 1. As shown in Fig. 2, the broad band can be divided into two peaks. It can be noted that both samples show a peak with lower energy than the free exciton emission, assuming it is a replica of the longitudinal optical (FX-1LO) phonon emitted by the free exciton, and the other is the optical (FX-2LO) phonon replica. In the Sa (F5428) sample, the energy difference between the two phonon peaks is about 73 meV; for the Sc (F5444) sample, the energy difference between the two phonon peaks is about 84 meV. Again the two phonon replica peaks are very close [32]. In the two samples studied here, the energy difference between the two phonon peaks of the Sc sample is larger than that of the Sa sample. One can also notice the intensity ratio of the FX-2LO peak and the FX-1LO peak of the film is different for two pieces of AlN. The ratio of Sc is obviously smaller than that of Sa. Therefore, we conclude that the crystal quality of the AlN film (Sc) grown on SiC is better than that of the AlN film (Sa) grown on sapphire. This phenomenon is caused by the lattice mismatch between the epitaxial film and the substrate and the thermal expansion coefficient mismatch between them.

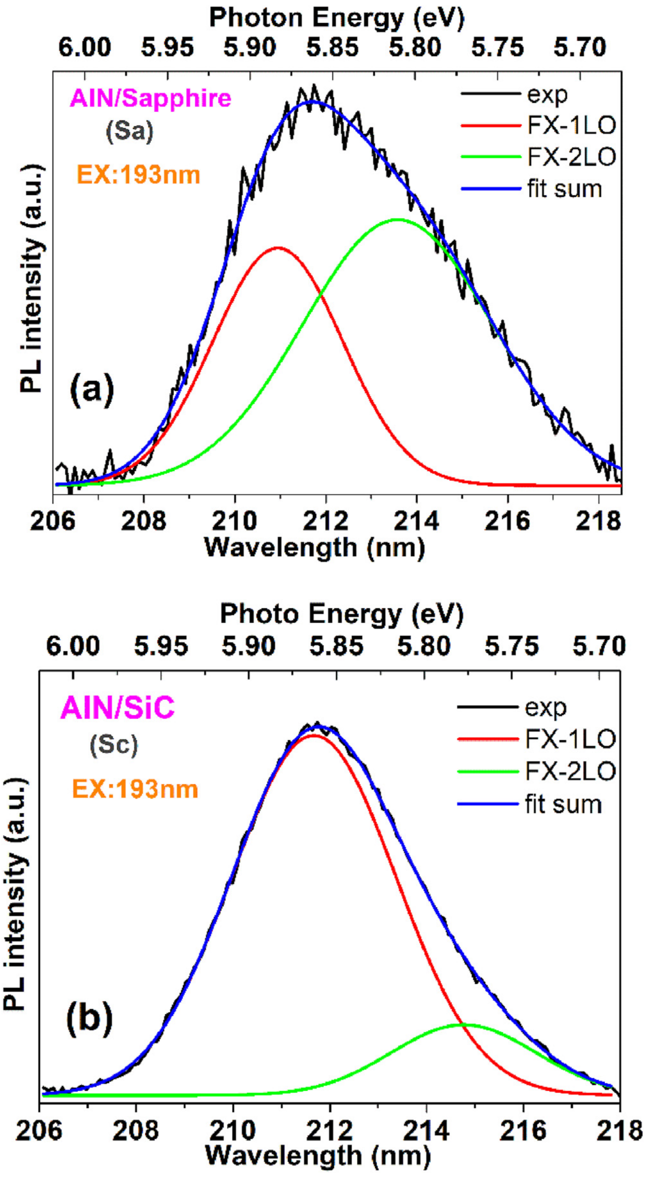

Fig. 2. Gaussian fitting of PL spectra excited by 193 nm, for (a) AlN/sapphire (Sa) and (b) AlN/6H–SiC (Sc), respectively.

3.1.2. XRD data

The HR-XRD is an effective method to understand not only the crystal structure and quality but also to identify its secondary phases. Fig. 3 (a) shows 2 scans for AlN film grown on two substrates from 25° to 140° . The HR-XRD patterns between the two aluminum nitride films show strong first-order aluminum nitride diffraction peaks (0002) and second-order aluminum nitride diffraction peaks (0006). The intensities of the first-order diffraction peaks (0002) are the strongest, and the crystal is preferentially oriented in this direction. In terms of the diffraction intensity, we can see that the diffraction peak of sample Sa (F5428) is significantly weaker than that of Sc (F5444). Fig. 3 (b) presents the rocking curves for the (0002) orientation. Using Gaussian fitting, the full-width at half-maximum of the peak can be obtained. For the Sa and Sc samples these are 0.130 arcsec and 0.067 arcsec, respectively – significantly smaller for the Sc (F5444) than the Sa (F5428) sample. Thus, for the two samples studied here, the crystal quality of the AlN film grown on Al_2O_3 substrate is inferior than that of prepared on 6H–SiC substrate. At the same time, we also estimated the average particle size of each sample by Debye-Sheller formula [33]:

Table 1
PL fitting parameter of 193 nm.

		Sa (**F5428**)		Sc (**F5444**)	
		Wavelength(nm)	Photon Energy(eV)	Wavelength(nm)	Photon Energy(eV)
FX-1LO	Peak position	210.945	5.878	211.669	5.858
	Height (**h$_1$**)	565.377		1875.213	
	FWHM	3.371		4.005	
FX-2LO	Peak position	213.583	5.806	214.764	5.774
	Height (**h$_2$**)	698.702		361.426	
	FWHM	4.925		3.517	
h$_2$/h$_1$		1.234		0.193	

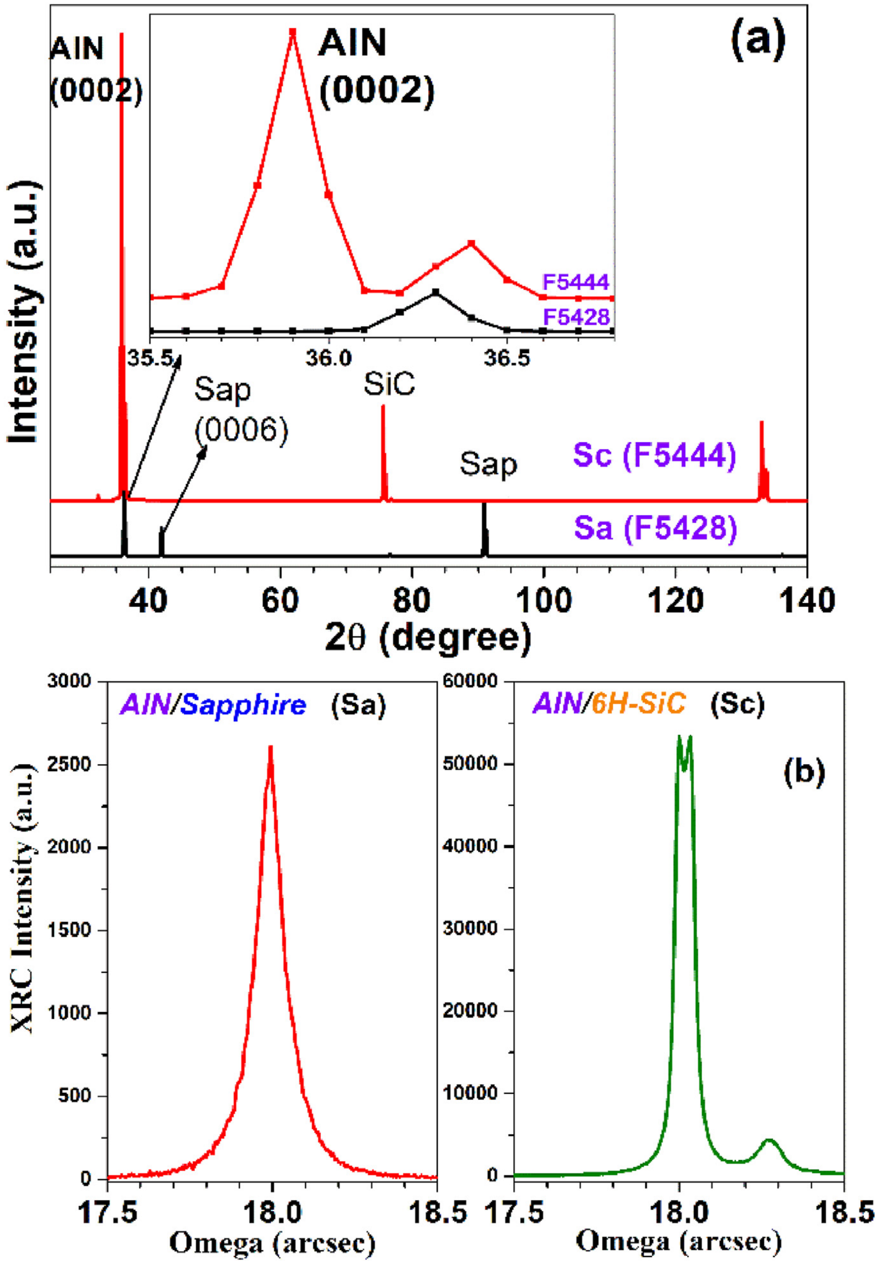

Fig. 3. (a) XRD pattern of AlN and (b) The (0002) plane XRC, of two AlN samples, respectively.

$$\mathrm{D} = \frac{K\lambda}{\beta \cos\theta} \tag{1}$$

where D: particle size (diameter), K: fixed parameter (film = 0.9), λ: $\mathrm{Cu}_{k\alpha}$ diffraction wavelength (0.15406 nm), β: half-peak width (FWHM(2θ)), θ: diffraction angle.

The detailed parameters extracted for AlN samples (Sa and Sc) are shown in the above Table 2a. It can be noted that the first-order diffraction peak angles of AlN films grown on different substrates are different – and certainly the film grown on Al_2O_3 is frailer than that on 6H–SiC. Also, it can be seen that the average grain diameter of the AlN film on the Al_2O_3 is smaller than that grown on 6H–SiC. According to the Bragg's equation 2dsin $\theta = \lambda(\mathrm{Cu}_{k\alpha})$ [23], d is the spacing between crystal planes, θ is the incident ray, the angle between the reflected line and the reflected crystal plane, and λ is the wavelength. It can be noted from the HR-XRD pattern that larger the 2θ angle – the smaller the interplanar spacing. In summary, comparing the AlN films on two different substrates we noticed that the interplanar spacing and crystal grain size of the AlN film grown on Al_2O_3 are smaller than the film grown on 6H–SiC substrate. Due to a smaller mismatch between AlN and 6H–SiC – the crystalline quality of the film improved significantly. Again, the AlN (0002) peaks of samples Sa (F5428) and Sc (F5444) appear at 36.29° and 35.90° , respectively. The diffraction angles of the two AlN films (0002) are slightly different, which can be interpreted from the lattice constant values of sapphire (a = 0.4785 nm, c = 1.2991 nm) [34] and 6H–SiC (a = 3.0730 Å, b = 10.053) [27] as well as AlN (a = 0.311 nm, c = 0.498 nm) [35]. In addition, the microscopic strain (Ɛ) can be calculated from the following expression [7]:

$$\varepsilon = \frac{\beta \cos\theta}{4} \tag{2}$$

with β:Full-width at half-maximum (FWHM(2θ))

The strain in AlN thin film grown on sapphire substrate is larger than that on SiC substrate. It is simply due to that the lattice mismatch (13%) of sapphire and AlN is greater than SiC (1%), and the coefficient of thermal expansion mismatch of sapphire ($7.7 \times 10^{-6}/^{\circ}$ C) and AlN ($4.6 \times 10^{-6}/^{\circ}$ C) is greater than SiC ($3.7 \times 10^{-6}/^{\circ}$ C) [36].

The dislocation density of AlN can be estimated by the following equation [18].

$$\delta = \frac{\beta^2_{(0002)}}{4.35b^2} \tag{3}$$

where b is the length of the Burgers vector (b = 0.3110 nm). The calculation of the above formula shows that the dislocation densities of the two samples of Sa (F5428) and Sc (F5444) are 0.46×10^{-3} nm^{-2} and 0.45×10^{-3} nm^{-2}, respectively.

From the results reported in Table 2b, the dislocation densities of the two samples are similar. The dislocation density of the aluminum nitride film grown on sapphire is slightly larger than that of the aluminum nitride film grown on silicon carbide. The magnitude of the strain is almost the same for two AlN films. It can be noticed that the sample with large thickness of aluminum nitride film have smaller dislocation density and micro-strain. The difference in the dislocation density of the two films may be due to the difference in thickness of the epitaxial layer. The AlN film with a large epitaxial layer thickness may form an adjacent dislocation loop opposite to the Burger vector direction [37]. Secondly, within these two AlN films, the thickness of the epitaxial layer on the sapphire substrate is smaller than that on the silicon carbide substrate, which can be attributed to the greater mobility of aluminum atoms on the sapphire substrate, and therefore, it can be used with for a shorter time on the lattice growth formation. Referring to the AFM results, the difference in grain size may be attributed to the bamboo shoot growth model of crystal growth [12]. These additional atoms may be trapped in twists, steps, or surface defects. Finally, we know that small dislocation density and large grain size indicate high sample crystallinity. Obviously, in the two AlN films studied, the crystal quality of Sc (F5444) is better than that of Sa (F5428).

Table 2a
detail parameters of AlN.

Sample	2θ(deg)	FWHM(deg)	Crystallite Size D (nm)	D nm (Average)
Sa (F5428)	36.29	0.17961	46.545	61.345
Sc (F5444)	35.90	0.1772	47.126	81.397

3.1.3. X-ray photoelectron spectroscopy (XPS)

Fig. 4(A) shows the full spectra of two aluminum nitride films and all XPS spectra were calibrated to the C1s peak at 284.8 eV. The XPS spectra confirmed that these AlN films are composed of aluminum, nitrogen, carbon, oxygen and other elements. Due to the influence of background, the Si peaks appearing nearby are not so obvious. The carbon peak may be caused by carbon-containing impurities adsorbed on the air or sample surface [38].

XPS fine scans of N1s and Al2p for two AlN films are exhibited in Fig. 4 (B). Here, the fitting software XPSPEAK 4.1 was used. Gaussian-Lorentz (20%–80%) function was used to fit the narrow spectra. The fitting results are shown in Table 3. By fitting the peaks of N1s and Al2p, two chemical states with different binding energies (B.E.) for aluminum and nitrogen can be obtained. One may note that all Al2p narrow spectra can be fitted into two sub-peaks of different chemical states. For the Sa (F5428) sample, the binding energy of Al–N is 73.576 eV and the binding energy of Al–O is 74.285 eV; for the Sc (F5444) sample, the binding energy of Al–N is 74.029 eV and the binding energy of Al–O is 75.358 eV. Similarly, all N1s narrow spectra can also be fitted into two sub-peaks with different chemical states. First look at the Sa sample, the binding energy of Al–N is 399.739 eV, the binding energy of N–O is 396.817 eV; secondly for the Sc sample, the binding energy of Al–N is 398.967 eV, and the binding energy of N–O is 398.447 eV. For the narrow-spectrum Al2p, it can be seen that the chemical binding energy of Sa is smaller than that of sample Sc. Factors such as charge transfer effects, the presence of electric fields, hybridization, and environmental charge density may all cause changes in binding energy. Among these factors, charge transfer is considered to be the main mechanism [39].

By fitting each sub-peak, using the sensitivity constant and the calculation formula, the thickness d(Å) of the surface oxide film can be estimated by

$$d_{xps}(\mathring{A}) = \lambda_0 \sin\theta \ln\left(\frac{N_m I_0 \lambda_m}{N_o I_m \lambda_0} + 1\right) \tag{4}$$

Among them, the ratio of the volume density of aluminum atoms to oxides in metal atoms is $N_m/N_0 = 1.6$ (calculated according to the density of Al = 2.7 g/cm^3 and $Al_2O_3 = 3.1$ g/cm^3, respectively), and λ_0 and λ_m are alumina and nitrogen, respectively. The attenuation length of aluminum oxide [40], θ is 75°, I_0/I_m is the ratio of the area of aluminum oxide to the area of aluminum nitride.

Oxygen contamination is easily formed on the surface of the film due to the high oxygen affinity of aluminum atoms [16]. It can be seen from the results in Table 3 that the thickness of the oxide film on the surface of the AlN film is different. The oxide film thickness

Table 2B
Calculation results of dislocation density and micro-strain of two aluminum nitride films.

Sample	Thickness (nm)	Dislocation density $\delta x10^{-3}$ (nm^{-2})	Micro strain $\varepsilon x10^{-3}$
Sa (**F5428**)	250.69	0.46	0.74
Sc (**F5444**)	675.62	0.45	0.73

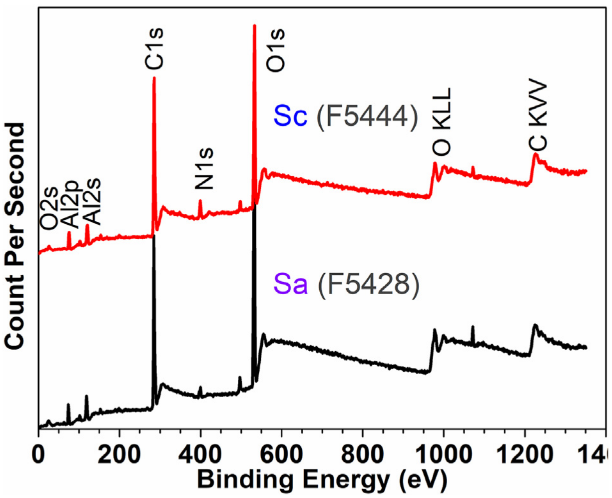

Fig. 4A. Wide-scan XPS spectra.

Table 3
XPS analysis result for the AlN thin films.

Film			Sa (F5428)	Sc (F5444)
Al2p	#1	B.E. (eV)	74.285	75.358
		FWHM (eV)	1.523	1.583
		Area	7211.044	9106.652
	#2	B.E. (eV)	73.576	74.029
		FWHM (eV)	1.351	1.618
		Area	5499.607	2519.232
N1s	#1	B.E. (eV)	399.739	398.447
		FWHM (eV)	1.913	1.021
		Area	6682.257	3472.049
	#2	B.E. (eV)	396.817	398.967
		FWHM (eV)	1.424	3.393
		Area	2919.851	13099.860
d_{xps}(Å) (nm)			28.19	49.26

of the AlN film on the 6H–SiC substrate is obviously thicker than that of the AlN film on the sapphire. This is due to the different oxygen affinity of the two films.

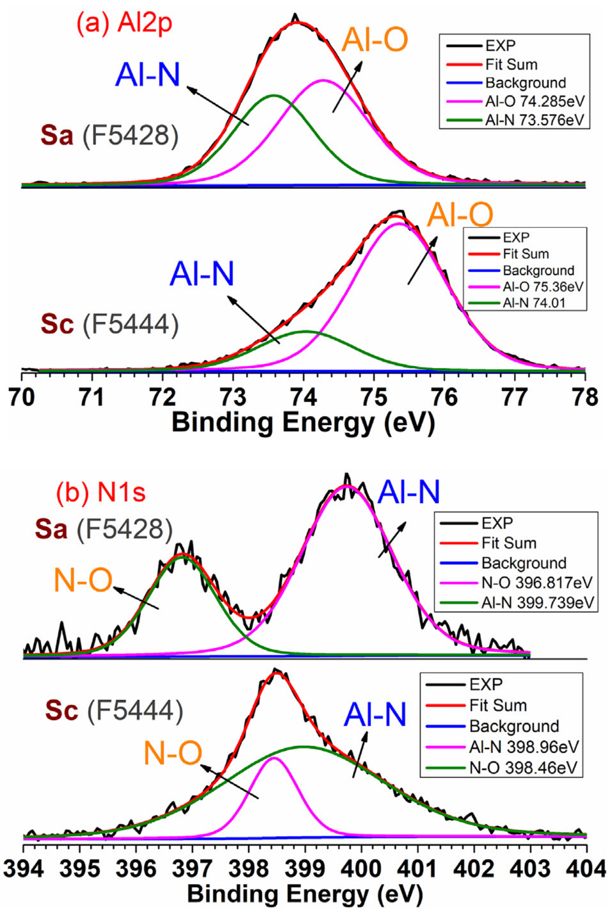

Fig. 4B. Fine-scan spectra of (a) Al2p and (b) N1s for two AlN films, respectively.

3.2. Optical characterization of AlN

3.2.1. Room temperature Raman scattering spectra

Fig. 5 shows the RS spectra of two aluminum nitride samples with different substrates excited by 266 nm and 532 nm lasers. The perusal of Fig. 5 reveals that when using 532 nm/266 nm excitation, the major Raman peaks of the AlN/Al_2O_3 film Sa (F5428) are located near 248.55 cm^{-1}, 656.94 cm^{-1}/661.37 cm^{-1} and 889.59 cm^{-1}/ 895.32 cm^{-1}respectively. On the other hand the Raman peaks of AlN/6H–SiC film Sc (F5444) are located near 266.71 cm^{-1}, 648.12 cm^{-1}/654.94 cm^{-1} and 886.62 cm^{-1}/889.57 cm^{-1}. These features correspond to the E_2(Low), E_2(high) and A_1(LO) of AlN film. Secondly, the half-width of the E_2 (high) of the RS spectrum of two samples, Sa and Sc, excited by two lasers can be obtained. For the excitation of 532 nm, the half-widths of Sa and Sc are 7.6 and 5.7 cm^{-1}, respectively; Excited at 266 nm, Sa and Sc have half-widths of 16.2 and 14.3 cm^{-1}, respectively. Obviously among the two samples, the crystal quality of Sc is better than that of Sa.

In the absence of stress, the Raman frequency position of the aluminum nitride E_2 (high) phonon mode is 657.4 ± 0.2 cm^{-1} [19]. From the Gaussian fit of RS spectrum with 266 nm excitation for the Sa sample, the Raman frequency position of the E_2 (high) phonon mode can be obtained as 661.3 cm^{-1} – the value is higher by 3.9 cm^{-1} with respect to the case of no stress – caused by compressive stress. For the Sc sample, the Raman frequency position of the E_2 (high) phonon mode is 654.9 cm^{-1}, with a Raman displacement of -2.5 cm^{-1} relative to the unstressed condition is caused by the tensile stress. Secondly for the Raman spectrum excited at 532 nm, one can also be obtained that the E_2(high) phonon mode Raman frequency positions of Sa and Sc are 656.9 cm^{-1} and 648.12 cm^{-1}, respectively, and the Raman displacements under unstressed conditions are -0.5 cm^{-1} and -9.28 cm^{-1}, respectively. This is due to the fact that the thermal expansion coefficient of aluminum nitride is greater than 6H–SiC, and the lattice mismatch between the substrate and the epitaxial layer results in tensile stress [41]. The following formula can be used to calculate the stress [20,42];

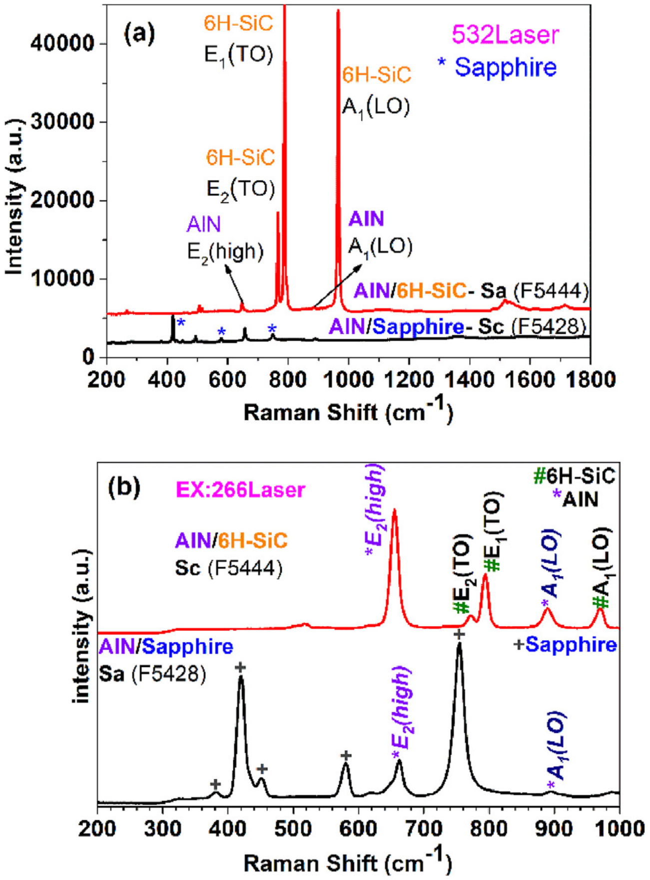

Fig. 5. Raman spectra excited by 532 nm laser and 266 nm laser for two AlN films.

$$\sigma = \Delta\omega / K \tag{5}$$

where $\Delta\omega$ is the difference between the E_2(high) phonon peak between the stressed and unstressed AlN epitaxial layer, and K (2.4 ± 0.2 cm^{-1}/GPa) is the strain coefficient.

3.2.2. Temperature-dependent Raman spectra

The results of temperature-dependent RS spectra between 80 K and 800 K for the two A_1(LO) and E_2 (high) modes of our samples are displayed in Fig. 6 (a) and (b), respectively. For AlN, we can evaluate the grain size and residual strain from the sum of the half-width of its E_2 (high) Raman mode. As the temperature increases, the decrease of the Raman mode is caused by thermal expansion and phonon-phonon interaction. As can be seen clearly from Fig. 6 (a1) and (b1), as the temperature increases, the Raman shift of the scattering peak gradually moves to a low wave number. Between 80 K and 800 K, for sample Sa (F5428), the E_2(high) mode shifts by about 16.3 cm^{-1} from Fig. 6 (b1), while for the Sc (F5444) sample, the E_2(high) mode moved about 10.1 cm^{-1} from Fig. 6 (a1). One may note from the low temperature to high temperature data, the Raman displacement of the aluminum nitride film grown on the sapphire substrate is larger than that grown on the silicon carbide substrate. The main reason for the displacement of the scattering peak may be (i) as the temperature gradually increases, the non-intermittent coupling between the phonons will gradually increase; (ii) the thermal expansion effect of the lattice. All the above reasons will lead to the change of lattice vibration energy level, which will cause the corresponding displacement of the corresponding Raman scattering peak frequency [12].

From the Gauss function fitting of E_2(high) mode, the Raman shift and FWHM-temperature curves are obtained. As shown in Fig. 7(A) and (B), the red and blue solid lines are the fitting Line, and one can see the relationship between the half-width and the Raman shift with temperature. As the temperature increases, the peak positions of the two samples slowly move to the low wave-number direction. The Raman shift of the AlN film grown on Al_2O_3 is relative to that prepared on 6H–SiC. To be closer to the fitted curve, the trend is closer to linear change. For the Raman FWHM of two aluminum nitride films, by fitting the curve, as the temperature increases, they all decrease first, and then gradually increase. The temperature at which the Raman FWHM of the two aluminum nitride films changes. The inflection point is different. The temperature inflection point of aluminum nitride film Sa (F5428) on sapphire is 440 K; while the temperature inflection point of aluminum nitride film Sc (F5444) on 6H–SiC is 200 K. Secondly, regarding the movement of Raman frequency and the widening of FWHM temperature, according to the perturbation theory [12], the movement of Raman frequency is mainly due to its thermal expansion effect and the non-harmonic coupling between the an-harmonic vibration of the lattice point and the phonon caused. The FWHM temperature broadening effect mainly comes from an-harmonic broadening, which comes from temperature-dependent phonon attenuation, that is, optical phonons decay into low-energy phonons. Therefore, we can get the phenomenon that the Raman shift of the E_2(high) mode gradually shifts to a low wave number as the temperature rises and is attributed to the thermal expansion and an-harmonic vibration effects.

Fig. 8 is the change curve of the stress of two AlN films with temperature. The Raman spectra excited by a 266 nm laser were used, and the stress can be obtained by the above formula. It can be seen from the blue circles and blue fitting curve in Fig. 8 that for the AlN film grown on the Al_2O_3 substrate, in the temperature range of 80 K–600 K, the biaxial compressive stress of the AlN film decreases with the increase of temperature. But, within the range of 600 K–800 K, the biaxial stress of AlN film is changed to negative, i.e. becomes to tensile stress, which continue to increase in absolute value with the increase of temperature. In other hands, for the AlN film grown on the 6H–SiC substrate, in the temperature range of 80 K–250 K, the biaxial compressive stress of the AlN film decreases with the increase of temperature; in the range of 250 K–800 K, the biaxial stress of AlN film was changed to biaxial tensile stress, which further gradually increases in amount with the increase of temperature. It is found interestingly that at a certain temperature point, their biaxial stress changes from compressive stress to tensile stress. However, the changing points in temperature of the two aluminum nitride films are different, and it is higher for AlN grown on the sapphire substrate that on SiC substrate. The stress mutation temperature of aluminum nitride film is 600 K; while the stress mutation temperature of AlN film grown on 6H–SiC is 250 K. This may be caused by the difference between the thermal expansion coefficients of sapphire, 6H–SiC and aluminum nitride.

3.2.3. 3 optical transmission measurement (OT)

Fig. 9 is the transmission spectrum of the AlN thin film on sapphire. The transmittance can be obtained by removing the measured experimental spectrum from the single-sided polished sapphire substrate. Obviously, the AlN film shows a clear absorption edge between 200 nm and 227 nm, and the vibration above the absorption edge of the sample can also be observed, indicating that the sample has good crystalline quality. The optical transmittance of AlN film is greater than 70% in the UV band (200–400 nm). It can be seen that its band gap is around 199 nm (6.22 eV). The relationship between transmittance and E_g can be obtained from [43].

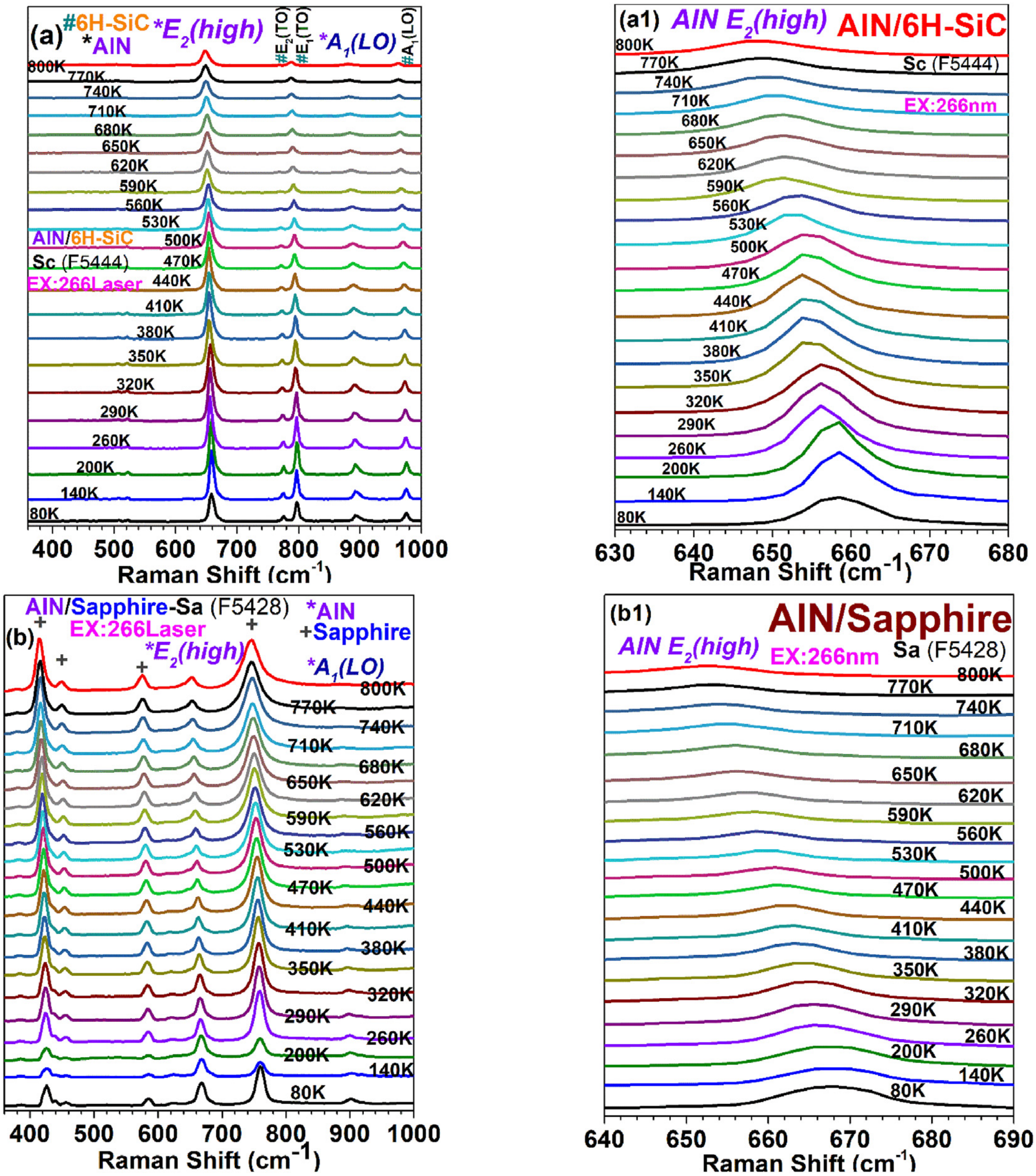

Fig. 6. (a, a1, b, b1). 266 nm laser excited temperature-dependent Raman spectra.

$$\alpha = \left(\frac{1}{t}\right) \times [\ln(T\%)] \tag{6}$$

$$(\alpha h\nu)^{\frac{1}{2}} = h\nu - E_g \tag{7}$$

where α is the absorption coefficient, t is the film thickness, T% is the transmittance, $h\nu$ is the photon energy, and E_g is the band gap energy [44]·

3.2.4. Spectroscopic ellipsometry (SE)

Spectroscopic ellipsometry (SE) measures the changes in polarization states psi (ψ) and delta (Δ) between incident and reflection of light on a sample. It can be used to accurately evaluate optical constants, layer thickness and surface roughness. By using a dual-rotation compensator, the ellipsometric spectra of the wavelength range (195 nm–1600 nm) were measured for two samples, as shown in Fig. 10, including fits described below. The optical constants and band gap can be fitted to the ellipse spectrum through a suitable theoretical model. According to the structural characteristics of the AlN sample, the physical model of roughness/oxide layer/AlN layer/substrate is used. The substrate uses Al_2O_3 and 6H–SiC respectively, and remains fixed during the entire fitting process. In order to obtain the thickness of the AlN epitaxial layer, the Caughy dispersion model is used to fit the transparent area, the formula is:

$$n(\lambda) = A + B\big/\lambda^2 + C\big/\lambda^4 \tag{8}$$

$$k(\lambda) = \alpha_0 e^{\beta(1.24\mu m(1/\lambda - 1/\gamma))} \tag{9}$$

where n is the refractive index, k is the extinction coefficient, A, B, and C are the fitting parameters, α_0 is the extinction coefficient amplitude, β is the exponential factor, and γ is the band edge [21,45–47]. The thickness of the AlN epitaxial layer and the initial

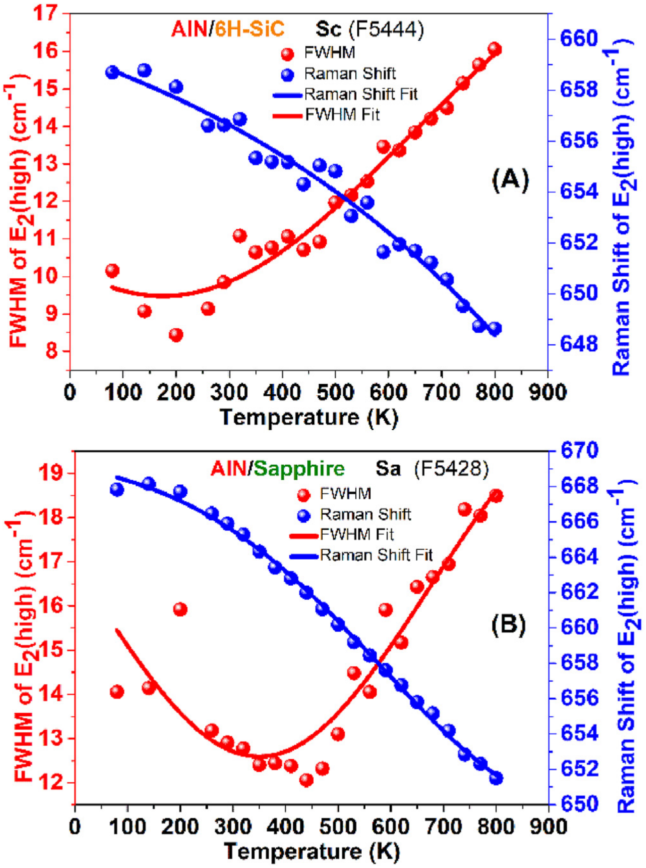

Fig. 7. (A)–(B). Raman linewidth and shift of E_2(high) as a function of temperature.

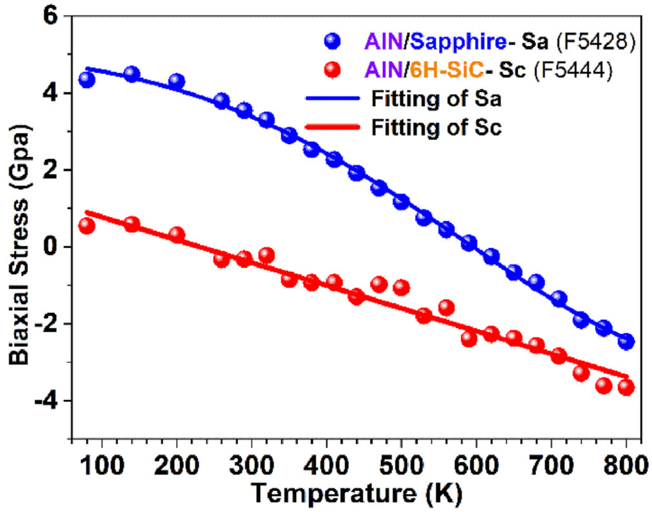

Fig. 8. The dependence of stress in AlN film on temperature.

value of the surface roughness can be determined in this fitting stage. Secondly, according to XPS, we can find that there is an oxide layer on the surface, and use the Caughy model to fit the surface oxide layer to get its initial value.

For Sa (F5428), we used B-Spline to further fit the best initial value obtained by Caughy model. By setting the wavelength range, the wavelength range is slowly expanded to the absorption spectrum range, and the range pushed to the high energy end is further shortened each time near the band gap, so that it has a denser energy node to better describe the excitons of AlN effect. Two Tauc-Lorentz Oscillators are used to further parameterize the dielectric function obtained by B-Spline [32]. Finally, by adjusting all the

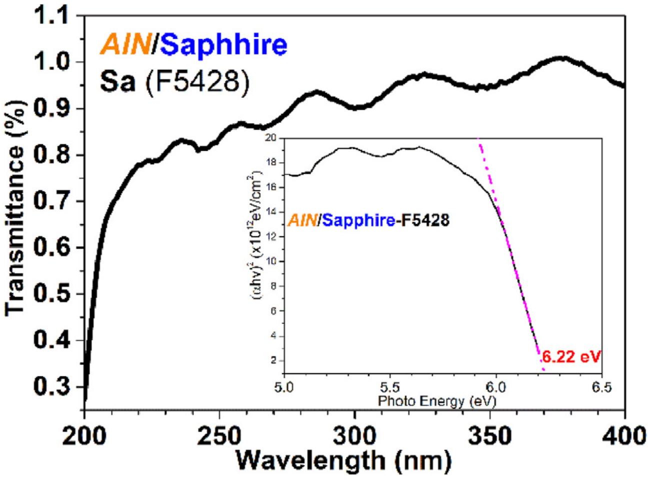

Fig. 9. Optical Transmittance spectra of AlN/sapphire, Sa (F5428).

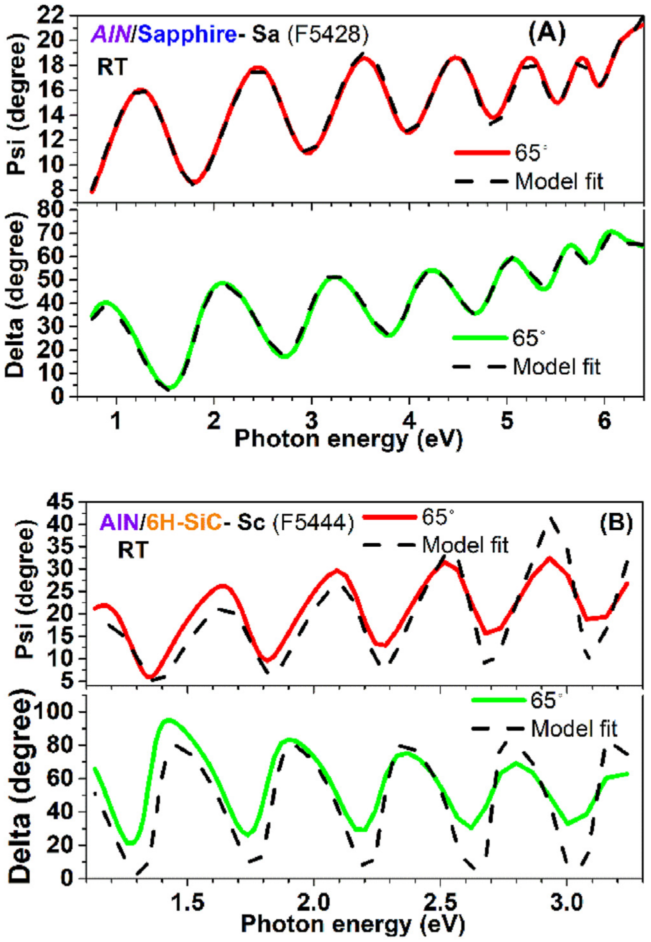

Fig. 10. SE room temperature (RT) experimental data (color solid lines) and model fitting results (black dashed lines) for sample (A) Sa (F5428) and (B) Sc (F5444). (For interpretation of the references to color in this figure legend, the reader is referred to the Web version of this article.)

parameters, thickness and surface roughness in the parametric model of the surface oxide layer and AlN layer, the fitting result with the mean square error (MSE) lower than 9 was obtained for the film sample. For Sc, due to the particularity of the substrate, the software used does not have a 6H—SiC model, only Cauchy fitting is performed on its transparent area, and its thickness is obtained. Fig. 11 shows the fitted results for the relationship of refractive index (n) and extinction coefficient (k) with photon energy for AlN film on sapphire, Sa (F5428).

The AlN film thicknesses of 251 nm for Sa and 676 nm for Sc, obtained by SE fittings, are shown in Table 2b. In the SE fitting results of Sa from Fig. 11, the band gap is 5.90 eV, which is a good verification of the PL test results; also the roughness and the thickness of the surface oxide film are 14.51 nm and 26.11 nm, respectively, basically consistent with the results obtained by AFM and XPS.

Previously, G. Shukla et al. [48] studied AlN thin films deposited on sapphire via pulsed laser deposition technique at room temperature, characterized by using cross-section SEM and other tools. J.H. O'Connell et al. [49] performed the defect characterization of MOCVD grown AlN/AlGaN films on sapphire substrates, by using nice cross-section TEM/STEM, FTIR reflectance and so on. We have also performed cross-section TEM/FTIR comparative studies for GaN/sapphire [50,51]. Current determination of AlN film thickness via SE and simulation is good (and convenient to us), compatible to above cited studies [48–51].

It can be noted that the band gap obtained by OT is significantly larger than that obtained by PL and SE. From equations (1) and (2), this may be because for films with small or thinner absorption coefficients, the absorption coefficient is often difficult to accurately measure through optical transmittance, and the thickness of most substrates is usually much larger than the thickness of the epitaxial layer, which may seriously hinder and interfere with the transmittance measurement of light. Therefore, the band gap value obtained by PL and SE has higher accuracy than the band gap value obtained by OT.

4. Surface analysis

Fig. 12 shows two AFM graphs of two samples of AlN grown on Al_2O_3 and 6H—SiC substrates, which were measured with an area size of 4 μm × 4 μm. The image shows that the surface consists of randomly oriented nanoparticle structures. Using NanoScope Analysis software for analysis, one can get its 3D maps, and analyze the surface roughness and particles. From its 3D image, it can be found that the surface of the aluminum nitride film Sa (F5428) grown on sapphire has an island-like morphology, and the surface of the aluminum nitride film Sc (F5444) grown on silicon carbide substrate has a bamboo shoot morphology [52]. Using NanoScope

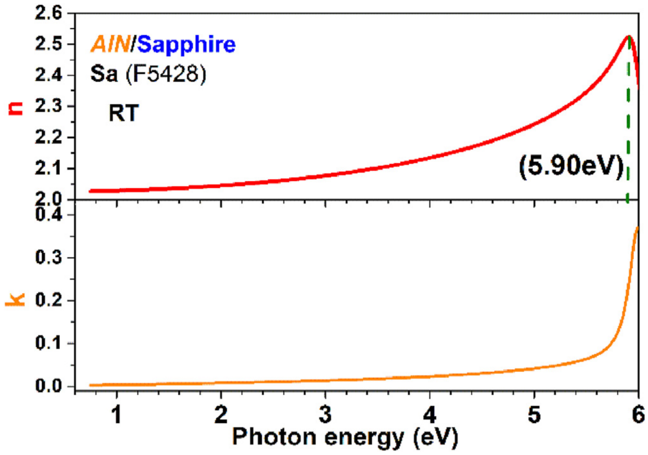

Fig. 11. Variation curves of refractive index (n) and extinction coefficient (k) of AlN film on sapphire, Sa (F5428), with Photon energy.

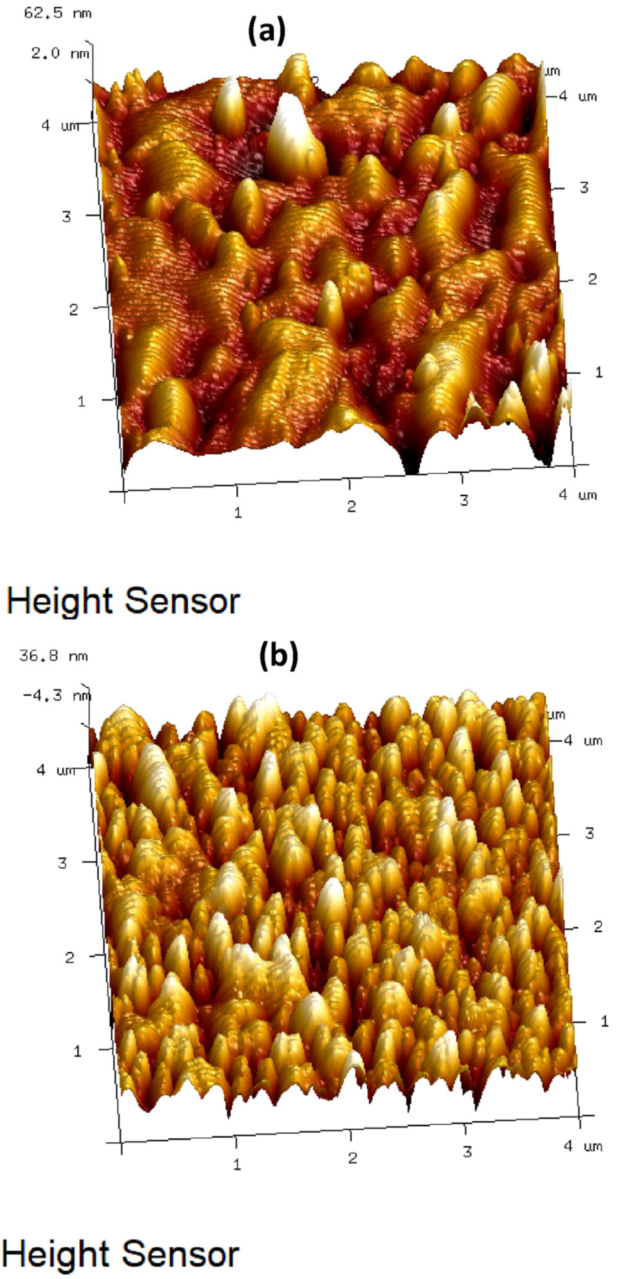

Fig. 12. 4 × 4 μm AFM diagram of two aluminum nitride films.

Table 4
Surface roughness and particle evaluated by AFM software analysis.

Sample	Roughness [nm]
Sa (F5428)	11.1
Sc (F5444)	8.89

for analysis, the surface roughness can be obtained and recorded in Table 4. It is obvious that the surface roughness of Sa sample is larger than that of Sc, and the surface size particles of Sa are smaller than those of Sc. The results show that the difference of the aluminum nitride film substrate may affect the roughness of the sample surface and the crystal particle size. Secondly, the grain size of the Sa sample is uneven, and the arrangement is not dense enough, and the surface is uneven. Compared with the Sa sample, the crystal quality of the Sc sample is better.

5. Conclusions

The surface, structure and optical properties of aluminum nitride films grown on sapphire and silicon carbide substrates were comprehensively studied. A series of important results have been achieved.

1. By analyzing the PL spectra of extreme deep ultraviolet (193 nm), the luminescence peak of the aluminum nitride film grown on the sapphire substrate is slightly lower in energy than that of the aluminum nitride film grown on silicon carbide substrate (redshift). Carrying out Gaussian fitting analysis and comparing the value of defect luminescence – the aluminum nitride film grown on sapphire substrate is larger – indicating the presence of defects causing deterioration of the film quality than those grown on silicon carbide substrate. This is due to the mismatch in lattice constants of epilayer and substrate as well as differences in their thermal expansion coefficients.
2. The AlN film grown on two different substrates was found to be dominated by the AlN (0002) plane. Secondly, a relative comparison was made between the two AlN films. Silicon carbide substrate provides better results for the growth of AlN film. The substrate can reduce the lattice mismatch between the aluminum nitride epitaxial layer and the substrate and improve the crystallinity.
3. The thickness of the aluminum nitride film grown on the sapphire and silicon carbide substrates was determined. The difference in thickness of the aluminum nitride film comes from different growth mechanisms and different mobility of Al atoms. The thicker aluminum nitride film grown on the silicon carbide substrate exhibits larger grain size, smaller micro-strain, smaller dislocation density and better crystal quality.
4. From XPS analysis, it can be found that there is an oxide layer on the surface of aluminum nitride. The thickness of the oxide layer on the surface of aluminum nitride grown on the silicon carbide substrate is thicker than that on sapphire. The former is almost the latter doubled, which is due to the different adsorption capacity of oxygen. The reason for this difference can be attributed to the variance of the oxygen affinity of aluminum atoms on different substrates. The oxygen affinity of AlN films grown on silicon carbide substrates is significantly higher than that of AlN films grown on sapphire substrates. .
5. Raman spectra excited by 266 nm and 532 nm lasers can clearly observe the E_2 (high) phonon mode. Comparing the half-width between them, it is identified that the crystal quality of the AlN film grown on the 6H–SiC substrate is better than the AlN film grown on sapphire. There exists a bi-axial stress in the aluminum nitride layer hetero-epitaxial on foreign substrate. The AlN film grown on silicon carbide substrate shows compressive stress, and the aluminum nitride grown on sapphire substrate shows tensile stress, in most cases.
6. Using the variable-temperature (VT) Raman spectroscopy excited by 266 nm, the Raman shift of the scattering peak gradually shifts from 80K–800K to a low wave number. The Raman shift of the aluminum nitride film grown on sapphire substrate is larger than that on silicon carbide substrate. Also, the peak width of the Raman scattering peak of the E_2(high) mode gradually widens. It is interesting to reveal from VT-RS data analyses that the biaxial stress existed in AlN films changes from compressive to tensile as temperature increases in the range of 80K–800K. The changing point for AlN/sapphire is higher than that of AlN/6H–SiC.
7. It can be seen from the optical transmission (OT) measurements that the transmittance of the aluminum nitride film grown on sapphire substrate can reach 70%, which has a good crystal quality. From the spectroscopic ellipsometry (SE) measurements and analyses, the thickness, roughness, band gap, and thickness of the surface oxide layer, for the AlN film grown on sapphire substrate were determined to be 250.69 nm, 14.51 nm, 5.90 eV, and 26.11 nm, respectively. The thickness of the AlN film on the 6H–SiC substrate is 675.62 nm.
8. The surface morphology measurements have revealed that the surface of the aluminum nitride film grown on sapphire has an island shape, and the surface of the aluminum nitride film grown on 6H–SiC has a bamboo shoot shape. The surface roughness of the former is greater than that of the latter, and the crystal quality is worse than that of the latter.
9. Our comprehensive work could provide a good reference for the further studies of the surface and optical properties of AlN heterostructures and related materials.

Declaration of competing interest

The authors declare that there is no conflict of interest.

Acknowledgments

This work was supported by the National Natural Science Foundation of China (No. 51868002), and the project supported by State Key Laboratory of Luminescence and Applications (No.SKLA-2019-06).

References

[1] Y. Zhu, R. Lin, W. Zheng, J. Ran, F. Huang, Near vacuum-ultraviolet aperiodic oscillation emission of AlN films, Sci. Bull. 65 (2020) 827–831, https://doi.org/10.1016/j.scib.2020.02.018.

[2] R. Supruangnet, W. Sailuam, W. Busayaporn, C. Wattanawikkam, A. Jiamprasertboon, A. Ruangvittayanon, W. Sangsai, A. Pirasampansiri, S. Limpijumnong, R. Yimnirun, A. Bootchanont, Effects of N2-content on formation behavior in AlN thin films studied by NEXAFS: theory and experiment, J. Alloys Compd. 844 (2020) 156128, https://doi.org/10.1016/j.jallcom.2020.156128.

[3] F. Dong, R. Li, G. Wu, K. Liang, G. Li, Y. Nie, Z. Gan, Q. Cao, X. Wang, Q. Zhao, S. Liu, An investigation of aluminum nitride thin films patterned by femtosecond laser, Appl. Phys. Lett. 116 (2020) 154101, https://doi.org/10.1063/5.0005183.

[4] R.D. Cong, J.M. Wang, X.Y. Wang, Y.F. Zhang, W.B. Lu, W. Zhao, Q.S. Wang, X.Y. Liu, W. Yu, Ferromagnetic anisotropy in scandium-doped AlN hierarchical nanostructures, J. Mater. Sci. 55 (2020) 8325–8336, https://doi.org/10.1007/s10853-020-04588-5.

[5] Hisashi Yoshida, Shigeya Kimura, High-crystalline-quality AlN grown on SiC substrates by controlling growth mode, J. Cryst. Growth 537 (2020) 125605, https://doi.org/10.1016/j.jcrysgro.2020.125605.

[6] S.-Y. Lin, F. Wu, C.-Q. Chen, Y. Liang, L.-Y. Wan, Z.-C. Feng, Temperature-dependent optical properties of AlN films characterized by spectroscopic ellipsometry, J. Infrared Millim. Waves 36 (2017) 276, https://doi.org/10.11972/j.issn.1001-9014.2017.03.005. +.

[7] Y. Li, C. Zhang, X. Luo, Y. Liang, D.-S. Wuu, C.-C. Tin, X. Lu, K. He, L. Wan, Z.C. Feng, Surface, structural and optical properties of AlN thin films grown on

different face sapphire substrates by metalorganic chemical vapor deposition, Appl. Surf. Sci. 458 (2018) 972–977, https://doi.org/10.1016/j.apsusc.2018.07.138.

[8] M.N. Abd Rahman, A.F. Sulaiman, M. Khudus, K. Allif, N.A. Talik, S.H. Basri, A. Shuhaimi, Effects of pulse cycle number on the quality of pulsed atomic-layer epitaxy AlN films grown via metal organic chemical vapor deposition, Jpn. J. Appl. Phys. 58 (2019) SC1037, https://doi.org/10.7567/1347-4065/ab09d3.

[9] W. Zheng, R.S. Zheng, H.L. Wu, F. Di Li, Strongly anisotropic behavior of A(1)(TO) phonon mode in bulk AlN, J. Alloys Compd. 584 (2014) 374–376, https://doi.org/10.1016/j.jallcom.2013.09.102.

[10] T. Oto, R.G. Banal, K. Kataoka, M. Funato, Y. Kawakami, 100 mW deep-ultraviolet emission from aluminium-nitride-based quantum wells pumped by an electron beam, Nat. Photon. 4 (2010) 767–771, https://doi.org/10.1038/nphoton.2010.220.

[11] B.D. Liu, Y. Bando, A.M. Wu, X. Jiang, B. Dierre, T. Sekiguchi, C.C. Tang, M. Mitome, D. Golberg, 352 nm ultraviolet emission from high-quality crystalline AlN whiskers, Nanotechnology 21 (2010) 7, https://doi.org/10.1088/0957-4484/21/7/075708.

[12] H.L. Wu, W. Zhao, C.G. He, K. Zhang, L.F. He, Z.T. Chen, Growth of high quality AlN/sapphire templates with high growth rate using a medium-temperature layer, Superlattice. Microst. 125 (2019) 343–347, https://doi.org/10.1016/j.spmi.2018.12.008.

[13] B. Tang, H.P. Hu, H. Wan, J. Zhao, L.Y. Gong, Y. Lei, Q. Zhao, S.J. Zhou, Growth of high-quality AlN films on sapphire substrate by introducing voids through growth-mode modification, Appl. Surf. Sci. 518 (2020) 146218, https://doi.org/10.1016/j.apsusc.2020.146218.

[14] J. Nomoto, T. Tsuchiya, T. Yamamoto, Well-defined (0001)-oriented aluminum nitride polycrystalline films on amorphous glass substrates deposited by ion plating with direct-current arc discharge, Appl. Surf. Sci. 478 (2019) 998–1003, https://doi.org/10.1016/j.apsusc.2019.02.027.

[15] F. Li, L. Wang, W. Yao, Y. Meng, S. Yang, Z. Wang, Analysis of growth rate and crystal quality of AlN epilayers by flow-modulated metal organic chemical vapor deposition, Superlattice. Microst. 137 (2020) 106336, https://doi.org/10.1016/j.spmi.2019.106336.

[16] L. Vergara, M. Clement, E. Iborra, A. Sanz-Hervas, J. Garcia-Lopez, Y. Morilla, J. Sangrador, M.A. Respaldiza, Influence of oxygen and argon on the crystal quality and piezoelectric response of AlN sputtered thin films, Diam. Relat. Mater. 13 (2004) 839–842, https://doi.org/10.1016/j.diamond.2003.10.063.

[17] C.-M. Lin, W.-C. Lien, V.V. Felmetsger, M.A. Hopcroft, D.G. Senesky, A.P. Pisano, AlN thin films grown on epitaxial 3C–SiC (100) for piezoelectric resonant devices, Appl. Phys. Lett. 97 (2010) 141907, https://doi.org/10.1063/1.3495782.

[18] W. Luo, L. Li, Z. Li, Q. Yang, D. Zhang, X. Dong, D. Peng, L. Pan, C. Li, B. Liu, R. Zhong, Influence of the nucleation layer morphology on the structural property of AlN films grown on c-plane sapphire by MOCVD, J. Alloys Compd. 697 (2017) 262–267, https://doi.org/10.1016/j.jallcom.2016.12.126.

[19] M.N. Abd Rahman, A.F. Sulaiman, M.I.M.A. Khudus, K. Allif, N.A. Talik, S.H. Basri, A. Shuhaimi, Effects of pulse cycle number on the quality of pulsed atomic-layer epitaxy AlN films grown via metal organic chemical vapor deposition, Jpn. J. Appl. Phys. 58 (2019) SC1037, https://doi.org/10.7567/1347-4065/ab09d3.

[20] X. Rong, X. Wang, G. Chen, J. Pan, P. Wang, H. Liu, F. Xu, P. Tan, B. Shen, Residual stress in AlN films grown on sapphire substrates by molecular beam epitaxy, Superlattice. Microst. 93 (2016) 27–31, https://doi.org/10.1016/j.spmi.2016.02.050.

[21] Y. Liu, E. Ghafari, X. Jiang, Y. Feng, Z.C. Feng, I. Ferguson, N. Liu, Temperature-dependent optical properties of AlN thin films by spectroscopy ellipsometry, Mrs Advances 2 (2017) 323–328, https://doi.org/10.1557/adv.2017.171.

[22] B. Tang, H. Hu, H. Wan, J. Zhao, L. Gong, Y. Lei, Q. Zhao, S. Zhou, Growth of high-quality AlN films on sapphire substrate by introducing voids through growth-mode modification, Appl. Surf. Sci. 518 (2020) 146218, https://doi.org/10.1016/j.apsusc.2020.146218.

[23] Y. Qi, Y. Wang, Z. Pang, Z. Dou, T. Wei, P. Gao, S. Zhang, X. Xu, Z. Chang, B. Deng, S. Chen, Z. Chen, H. Ci, R. Wang, F. Zhao, J. Yan, X. Yi, K. Liu, H. Peng, Z. Liu, L. Tong, J. Zhang, Y. Wei, J. Li, Z. Liu, Fast growth of strain-free AlN on graphene-buffered sapphire, J. Am. Chem. Soc. 140 (2018) 11935–11941, https://doi.org/10.1021/jacs.8b03871.

[24] X.-H. Li, S. Wang, H. Xie, Y.O. Wei, T.-T. Kao, M.M. Satter, S.-C. Shen, P. Douglas Yoder, T. Detchprohm, R.D. Dupuis, A.M. Fischer, F.A. Ponce, Growth of high-quality AlN layers on sapphire substrates at relatively low temperatures by metalorganic chemical vapor deposition, Phys. Status Solidi 252 (2015) 1089–1095, https://doi.org/10.1002/pssb.201451571.

[25] V. Jindal, F. Shahedipour-Sandvik, Density functional theoretical study of surface structure and adatom kinetics for wurtzite AlN, J. Appl. Phys. 105 (2009), 075708, https://doi.org/10.1063/1.3106164.

[26] L. Liu, B. Liu, J.H. Edgar, S. Rajasingam, M. Kuball, Raman characterization and stress analysis of AlN grown on SiC by sublimation, J. Appl. Phys. 92 (2002) 5183–5188, https://doi.org/10.1063/1.1506195.

[27] N. Onojima, J. Suda, H. Matsunami, Lattice relaxation process of AlN growth on atomically flat 6H-SiC substrate in molecular beam epitaxy, J. Cryst. Growth 237 (2002) 1012–1016, https://doi.org/10.1016/s0022-0248(01)02118-2.

[28] Y. Li, W. Wang, X. Li, L. Huang, Y. Zheng, X. Chen, G. Li, Nucleation layer design for growth of a high-quality AlN epitaxial film on a Si(111) substrate, CrystEngComm 20 (2018) 1483–1490, https://doi.org/10.1039/c7ce02126g.

[29] L. Huang, Y. Li, W. Wang, X. Li, Y. zheng, H. Wang, Z. Zhang, G. Li, Growth of high-quality AlN epitaxial film by optimizing the Si substrate surface, Appl. Surf. Sci. 435 (2018) 163–169, https://doi.org/10.1016/j.apsusc.2017.11.002.

[30] J. Lemettinen, H. Okumura, I. Kim, M. Rudzinski, J. Grzonka, T. Palacios, S. Suihkonen, MOVPE growth of nitrogen- and aluminum-polar AlN on 4H-SiC, J. Cryst. Growth 487 (2018) 50–56, https://doi.org/10.1016/j.jcrysgro.2018.02.020.

[a] J. Lemettinen, H. Okumura, I. Kim, C. Kauppinen, T. Palacios, S. Suihkonen, MOVPE growth of N-polar AlN on 4H-SiC: Effect of substrate miscut on layer quality, J. Cryst. Growth 487 (2018) 12–16, https://doi.org/10.1016/j.jcrysgro.2018.02.013.

[31] Y. Zhu, W. Zheng, J. Ran, F. Huang, Deep-ultraviolet aperiodic-oscillation emission of AlGaN films, Optic Lett. 45 (2020) 1719–1721, https://doi.org/10.1364/ol.387256.

[32] Y. Liu, T. He, D. Chen, H. Yang, I.T. Ferguson, D. Huang, Z.C. Feng, Effects of annealing temperature, thickness and substrates on optical properties of m-plane ZnO films studied by photoluminescence and temperature dependent ellipsometry, J. Alloys Compd. 848 (2020) 156631, https://doi.org/10.1016/j.jallcom.2020.156631.

[33] E. Cetinorgu, S. Goldsmith, R.L. Boxman, The effect of annealing on filtered vacuum arc deposited ZnO thin films, Surf. Coating. Technol. 201 (2007) 7266–7272, https://doi.org/10.1016/j.surfcoat.2007.01.036.

[34] H.J. Kim, A. Duzik, S.H. Choi, Lattice-alignment mechanism of SiGe on sapphire, Acta Mater. 145 (2018) 1–7, https://doi.org/10.1016/j.actamat.2017.11.031.

[35] H.-C. Hsu, G.-M. Hsu, Y.-s. Lai, Z.C. Feng, S.-Y. Tseng, A. Lundskog, U. Forsberg, E. Janzen, K.-H. Chen, L.-C. Chen, Polarized and diameter-dependent Raman scattering from individual aluminum nitride nanowires: the antenna and cavity effects, Appl. Phys. Lett. 101 (2012) 121902, https://doi.org/10.1063/1.4753798.

[36] W.M. Yim, R.J. Paff, Thermal expansion of AlN, sapphire, and silicon, J. Appl. Phys. 45 (1974) 1456–1457, https://doi.org/10.1063/1.1663432.

[37] B.N. Pantha, R. Dahal, M.L. Nakarmi, N. Nepal, J. Li, J.Y. Lin, H.X. Jiang, Q.S. Paduano, D. Weyburne, Correlation between optoelectronic and structural properties and epilayer thickness of AlN, Appl. Phys. Lett. 90 (2007) 241101, https://doi.org/10.1063/1.2747662.

[38] H. Yang, Y. Qian, C. Zhang, D.-S. Wuu, D.N. Talwar, H.-H. Lin, J.-F. Lee, L. Wan, K. He, Z.C. Feng, Surface/structural characteristics and band alignments of thin Ga2O3 films grown on sapphire by pulse laser deposition, Appl. Surf. Sci. 479 (2019) 1246–1253, https://doi.org/10.1016/j.apsusc.2019.02.069.

[39] P. Motamedi, K. Cadien, XPS analysis of AlN thin films deposited by plasma enhanced atomic layer deposition, Appl. Surf. Sci. 315 (2014) 104–109, https://doi.org/10.1016/j.apsusc.2014.07.105.

[40] M.R. Alexander, G.E. Thompson, X. Zhou, G. Beamson, N. Fairley, Quantification of oxide film thickness at the surface of aluminium using XPS, Surf. Interface Anal. 34 (2002) 485–489, https://doi.org/10.1002/sia.1344.

[41] I.P. Nikitina, M.P. Sheglov, Y.V. Melnik, K.G. Irvine, V.A. Dmitriev, Residual strains in GaN grown on 6H-SiC, Diam. Relat. Mater. 6 (1997) 1524–1527, https://doi.org/10.1016/s0925-9635(97)00122-2.

[42] A. Kamarudzaman, A.S. Bin Abu Bakar, A. Azman, A.-Z. Omar, A. Supangat, N.A. Talik, Positioning of periodic AlN/GaN multilayers: effect on crystalline quality of a-plane GaN, Mater. Sci. Semicond. Process. 105 (2020) 104700, https://doi.org/10.1016/j.mssp.2019.104700.

[43] S.-L. Ou, D.-S. Wuu, Y.-C. Fu, S.-P. Liu, R.-H. Horng, L. Liu, Z.-C. Feng, Growth and etching characteristics of gallium oxide thin films by pulsed laser deposition, Mater. Chem. Phys. 133 (2012) 700–705, https://doi.org/10.1016/j.matchemphys.2012.01.060.

[44] T.Y. Lin, L. Li, C. Chen, Y.L. Chung, S.D. Yao, Y.C. Lee, Z.R. Qiu, I.T. Ferguson, D.S. Wuuf, Z.C. Feng, Material properties of MOCVD grown AlGaN layers influenced by indium-incorporation, in: M.H. Kane, C. Wetzel, J.J. Huang (Eds.), Eleventh International Conference on Solid State Lighting, 2011, p. 812309, 10.117/12.892932.

[45] C. Zhang, Y. Li, Y. Qian, Y. Liang, D.N. Talwar, S.-Y. Huang, Q. Li, D. Seidlitz, N. Dietz, D.-S. Wuu, I.T. Ferguson, X. Lu, L. Wan, K. He, Z.C. Feng, Surface and optical properties of indium-rich InGaN layers grown on sapphire by migration-enhanced plasma assisted metal organic chemical vapor deposition, Mater. Res. Express 6 (2019), 016407, https://doi.org/10.1088/2053-1591/aae4b5.

[46] Y. Qian, Y. Liang, X. Luo, K. He, W. Sun, H.-H. Lin, D.N. Talwar, T.-S. Chan, I. Ferguson, L. Wan, Q. Yang, Z.C. Feng, Synchrotron radiation X-ray absorption spectroscopy and spectroscopic ellipsometry studies of InSb thin films on GaAs grown by metalorganic chemical vapor deposition, Advances in Materials Science and Engineering 2018 (2018) 1–11, https://doi.org/10.1155/2018/5016435.

[47] Y. Liu, Q.X. Li, L.Y. Wan, B. Kucukgok, E. Ghafari, I.T. Ferguson, X. Zhang, S. Wang, Z.C. Feng, N. Lu, Composition and temperature dependent optical properties of AlxGa1-xN alloy by spectroscopic ellipsometry, Appl. Surf. Sci. 421 (2017) 389–396, https://doi.org/10.1016/j.apsusc.2017.01.309.

[48] G. Shukla, A. Khare, Dependence of N2 pressure on the crystal structure and surface quality of AlN thin films deposited via pulsed laser deposition technique at room temperature, Appl. Surf. Sci. 255 (2008) 2057–2062, https://doi.org/10.1016/j.apsusc.2008.06.190.

[49] J.H. O'Connell, M.E. Lee, J. Westraadt, J.A.A. Engelbrecht, Defect characterization of MOCVD grown AlN/AlGaN films on sapphire substrates by TEM and TKD, Physica B 535 (2018) 293–298, https://doi.org/10.1016/

j.physb.2017.08.005.

[50] Z.C. Feng, K. Li, Y.T. Hou, J. Zhao, W. Lu, W.E. Collins, A comparative study of high resolution transmission electron microscopy, atomic force microscopy and infrared spectroscopy for GaN thin films grown on sapphire by metal-organic chemical vapor deposition, Surf. Coating. Technol. 200 (2006) 3224–3229, https://doi.org/10.1016/j.surfcoat.2005.07.018.

[51] N. Devki, Talwar, hao-hsiung lin and Zhe chuan Feng, anisotropic optical phonons in MOCVD grown Si-doped GaN/sapphire epilayers, Mater. Sci. Eng., B 260 (2020) 114615_1–11461510, https://doi.org/10.1016/j.mseb.2020.114615.

[52] S. Subramani, M. Devarajan, Structural and surface analysis of chemical vapor deposited boron doped aluminum nitride thin film on aluminum substrates, Materials Science-Poland 37 (2019) 395–403, https://doi.org/10.2478/msp-2019-0056.